A Deep Learning Framework for Assessing the Risk of Transvenous Lead Extraction Procedures

Fazli Wahid[1], YingLiang Ma[1], Vishal Mehta[2], Sandra Howell[2], Steven Niederer[2, 3] and C. Aldo Rinaldi[2]

[1] School of Computing Sciences, University of East Anglia, UK
[2] School of Imaging Sciences and Biomedical Engineering, King's College London, UK
[3] National Heart and Lung Institute, Imperial College London, UK
f.wahid@uea.ac.uk

Abstract. This paper introduces a deep-learning framework augmented with human guidance for evaluating the risk associated with Transvenous Lead Extraction (TLE). TLE is one type of minimally invasive cardiac procedures, and it is to remove old pacing wires inside the heart. The deep-learning framework automatically extracts geometric features from a single plain chest X-ray image obtained before the procedure. It then utilizes these features in conjunction with clinical data to predict the procedural risk. All geometric features were recommended by a senior clinician and include the positions of coils, the number of leads inside the superior vena cava and the angle of leads. The proposed framework was trained and tested using a database comprising records from 1,053 patients who underwent TLE procedures. Notably, the framework was successfully trained despite the highly imbalanced nature of the data. An accuracy of 0.91 was achieved and the framework can predict 88% of major complication cases. By combining geometric features with clinical data, we were able to deliver a significantly better accuracy and a higher recall rate for detecting high-risks patients, when compared with existing approaches. The methodology described in this paper can be applied to the risk assessment for other cardiac procedures.

Keywords: Deep learning, Risk assessment, Geometric feature extraction.

1 Introduction

Transvenous lead extraction (TLE) is a minimally invasive cardiac procedure performed to remove implanted leads (wires) from the veins and heart. In recent decades, there has been widespread adoption of cardiac implantable electronic devices. As a result, an increasing number of patients may need lead extraction procedures due to various factors such as infection, lead malfunction, or the need for device upgrades [1]. While the success rate of the TLE procedure remains high, it can be complex and may result in severe complications, and in some cases, procedure-related death. Clinical studies conducted in European centers have reported a 1.7% rate of major complications including deaths [2]. Therefore, it is essential to assess the risk for each individual patient before the TLE procedure. Sidhu et al [3] has proposed an Electra Registry

Outcome Score (EROS) to create a risk assessment tool using a limited number of variables and an accuracy of 0.70 was achieved. Recently, Vishal et al [4] has trained three machine learning (ML) models and tested them on a ELECTRa database [3]. The best performing ML model is the logistic regression (accuracy: 0.74) and followed by the self-normalising neural network (0.73) and support vector machine (0.72). The results are marginally improvement from EROS.

We hypothesized that adding geometric features extracted from a plain chest X-ray image will further improve the accuracy. Therefore, a new deep-learning framework is created to extract geometric features from images and to be trained on two kinds of data inputs. One type of data is related to personal health conditions such as whether the patient has heart failure, chronic respiratory diseases or infected device as well as how long leads has been implanted and more. Those data have been used in previous ML models [4]. The other type of data is geometric features extracted from one plain chest X-ray image acquired before the procedure. The geometric features were first suggested by the senior clinician. Those features are the lead angulations at different locations, the coil position related to the superior vena cava (SVC) and the number of overlapping leads in the SVC. In this paper, robust computer vision algorithms were designed, which are based on deep learning techniques for image segmentation. The computer vision algorithms were able to automatically compute the positions of the leads or coils inside the X-ray image and derive other geometric information such as angulation. After conducting correlation tests between individual geometric features and the outcome of major complications, less significant geometric features were removed. Finally, the ML model was trained using the remaining geometric features along with data regarding personal health conditions.

The main contribution of this paper is the methodology for developing a deep learning framework that combines geometric features with other clinical data to achieve higher accuracy in detecting high-risk patients. The proposed approach is not limited to the TLE procedure using the chest X-ray image and it could apply to assess the risk of other cardiac interventional procedures using X-ray or CT images.

2 Automatic Object Detection

2.1 Selecting geometric features

From the existing literature [5] as well as the experiences from a senior clinician, four geometric features from the plain chest X-ray image were selected. As illustrated in figure 1, geometric features are the coil (thick wire) position related to the SVC, the number of leads in the SVC, the lead angulation near the entry point of the SVC and the angulation of the pacing lead in the right ventricle (RV). To determine the approximated location of the SVC inside the chest X-ray image, a generic anatomy model is overlaid with the chest X-ray image. From figure 2(a), the location of the SVC (green box) is the top left corner of the heart region (red box). The height of the green box is approximately half the height of the heart region. The width of the green box is approximately one third of the heart region. The method was verified by overlaying 3D

anatomy models (extracted from pre-procedure CT scan) with the chest X-ray image (figure 2b).

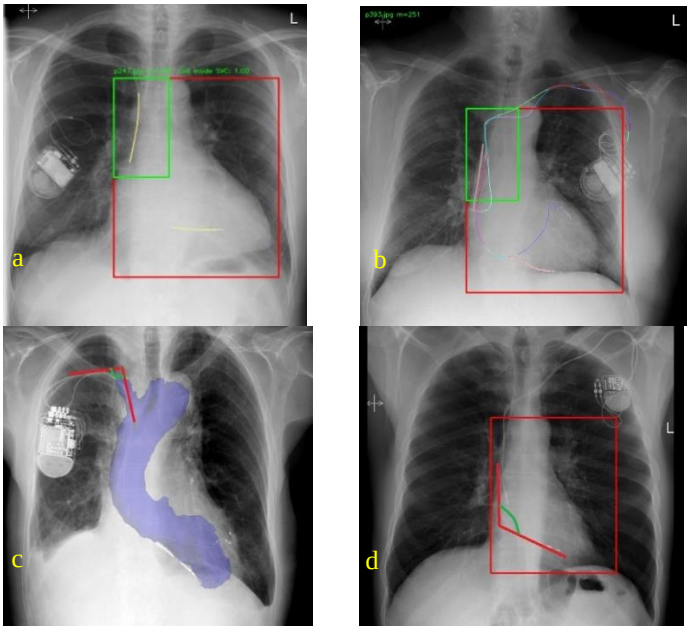

Fig. 1. The red box is the bounding box of the outline of the heart. The green box is the approximated location of the SVC. (a) The yellow lines are the positions of coils. (b) The colorful line segmentations inside the green box indicate how many wires are inside the SVC. (c) The angle formed by two red line is the lead angulation near the entry point of the SVC. The blue shadow represents the overlay of a heart model extracted from the CT images of the same patient. (d) The angle formed by two red line is the angulation of the pacing lead in the right ventricle.

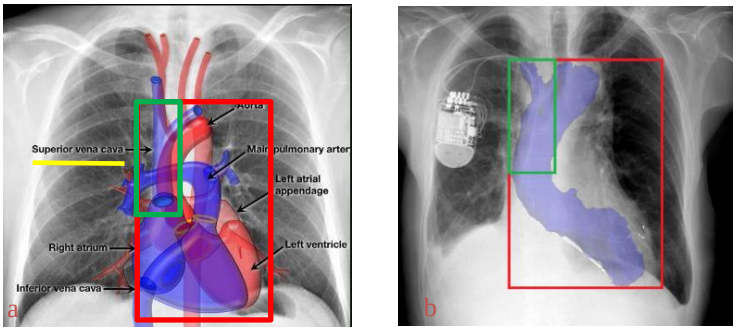

Fig. 2. (a) A medically accurate illustration of the anatomy of the heart. The red box is the region of the heart and the green box is the location of the SVC. (b) Overlaying 3D anatomy models with the X-ray image.

SVC is a major blood vessel inside the heart and it provides an important pathway for inserting the pacing leads into the right atrium and other heart chambers. The SVC is the most common location requiring surgical repair as the result of a major complication after the TLE procedure [5]. The common reason for the major complication inside SVC is the fibrotic tissue around the lead or the coil [10]. It does more likely happen to the coil which has a large surface area. The fibrotic tissue likely causes mechanical damages such as tear during the procedure.

2.2 The detection of the approximate location of SVC

To automatically located the SVC in the X-ray image, the heart region needs to be detected. A transfer learning approach was used to detect the heart region via bounding box regression, which is based on a modified VGG16 model. As shown in figure 3, the last 3 pre-trained fully-connected layers have been removed and replaced with 4 full-connected layers (128x1, 64x1, 64x1 and 4x1). The last layer outputs four float values, which are the coordinates of two corners positions of the bounding box. The modified VGG16 model uses the pre-trained weights (ImageNet) [6] and it was re-trained using the manual annotations of the heart region in X-ray images.

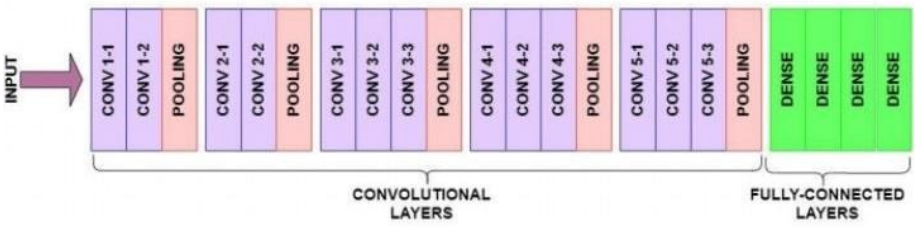

Fig. 3. The architecture of the modified VGG16 model.

Table 1. Results of precisions and recalls.

IoU Threshold	50%	75%
Precision	1.0	0.887
Recall	1.0	1.0

We have a database of 1,053 chest X-ray images from 1,053 patients and images were acquired before the TLE procedures. In addition, a public database of chest X-ray images [7] are also used and there are 5,863 images. The images from the public database were used solely to train and test the heart region detection method. They cannot be used for other detection or geometric feature extraction methods because they do not contain any pacing leads or coils. All images were split into two groups. 70% of images were used for training, 20% of images were used for validation and 10% of images were used for the accuracy testing. The bounding boxes of heart regions were manually annotated by a clinical expert. The loss function for the modified VGG16 model is the mean squared error (MSE) and the optimizer is adaptive moment estimation (Adam). The learning rate was set to 0.001. The accuracy of heart region detection is measured

by two metrics: precision and recall. Precision is the ability of a model to identify only the relevant objects. Recall is the ability of a model to find all ground truth bounding boxes. Both precision and recall were calculated at T(IoU)=0.5 and T(IoU)=0.75. IoU is the Intersection Over Union, which measures how well the prediction bounding box aligns with the ground truth box. Table 1 presents the result. Examples of IoU and approximate location of the SVC were presented in figure 4.

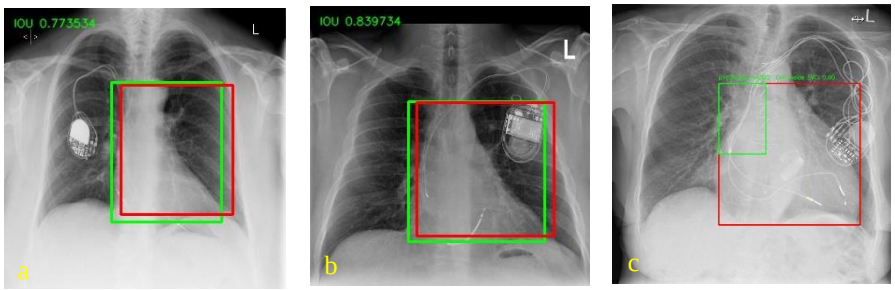

Fig. 4. Detecting the heart region. (a)(b) The results of IOU. The green box is the ground truth and the red box is the detected bounding box. (c) The green box is the bounding box of the SVC and the red box is the bounding box of the heart region.

2.3 The detection of pacing leads and coils

The next task to determine the position of pacing leads and coils. For the risk assessment, we categorized leads into two types of leads: the normal pacing lead and the pacing lead with coils. The normal leads are thin metal wires. On the other hand, the pacing lead with coils has one or two segments of coils. Coils have a large surface area of electrodes and they often conduct strong currents to depolarize the heart. They can be recognized on x-ray images as focal areas of wire thickening. The positions of pacing leads and coils in X-ray image need to be automatically localized in order to compute the position of coil, the number of normal pacing leads inside the SVC and the lead angulation. In order to achieve these tasks, a lightweight multiple-output convolutional neural network (MO-Net) based on the UNet-like architecture was proposed. MO-Net has two outputs. One is for the segmentation result and the other one is for localizing the tip position of the pacing lead inside the RV. The number of trainable parameters is 14.3M. Comparing to VGG16 (138M), AlexNet (62M) and ResNet-50 (23M), MO-Net is a lightweight network. As shown in figure 5, the main body of MO-Net is a UNet-like architecture, which consists of a downsampling path and an upsampling path. A box-regression branch starts at the bottom of UNet. The branch consists of a further convolution layer and two Max pooling layers to extract features and reduce the spatial dimensionality.

Both segmentation and box regression pathways share the same downsampling path, which consists of a series of convolution layers and Max pooling layers. There are two advantages to this approach. The first one is to reduce the computation load to achieve fast detection speeds. The convolution layers generate filters to extract features from the input image. As the segmentation and box regression targets the same objects,

similar features such as wire edges and corners will be extracted by convolution layers on the downsampling path. It is reasonable to allow the segmentation and box regression pathways to share a series of convolution layers so that the computation load is significantly reduced. The second advantage is to enable transfer learning. The MO-Net is trained on one type of target objects and it can be re-trained on another type of objects using transfer learning. The time of re-training could be significantly shortened if pre-trained weights (e.g. ImageNet) are loaded.

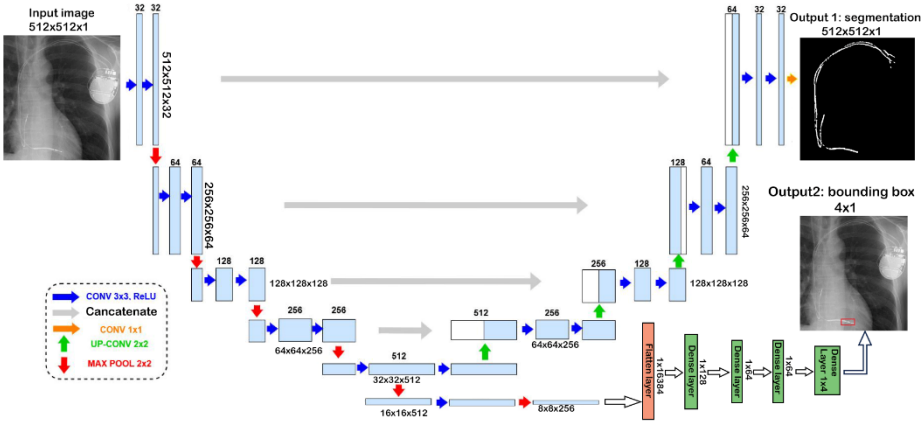

Fig. 5. The architecture of MO-Net.

Manual labeling. The manual labeling of pacing leads and wires in X-ray images is very time-consuming and tedious. To speed the process up, vessel enhancement filters [8] were used to extract catheters and wires. The resulting image was automatically binarized by an adaptive binarization method [9]. Not all wires were labeled in our training data. As we are only interested in pacing wires inside the heart, the pacemaker and nearby wire segments were also removed as they are not useful for finding geometric features. Therefore, an experienced clinician manually removed the non-target objects. Figure 6 presented the process of manual segmentation.

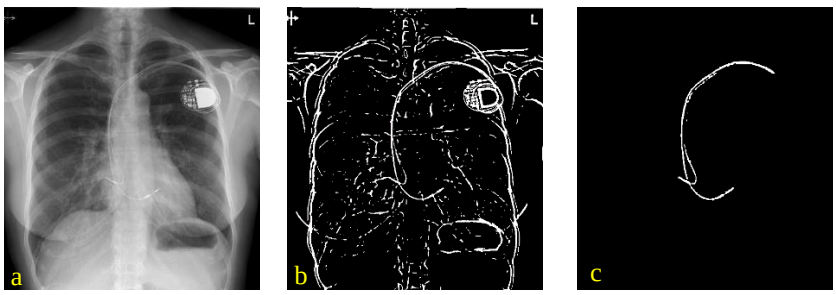

Fig. 6. Manual segmentation of pacing leads. (a) The original image. (b) Image after applying the vessel enhancement filter. (c) The final result of manual segmentation.

Training and results. The ratio for train-validation-test split is 7:2:1 and it is same as the ratio used in the detection of heart region. The loss function for the segmentation output is the dice similarity coefficient (DSC). The optimizer is Adam. The MO-Net was trained using 737 images. Images with the resolution of 512 × 512 were directly input into the network without any down-sampling as the leads might not be visible in the low resolution images. The data augmentation technique was used to increase the number of training images. The contrast or brightness of the 737 images were reduced by a random factor between 0.6 to 0.9 to create additional 1,474 training images. The reason for reducing contrast or brightness is to improve the performance of coil detection for low-contrast or dark X-ray images. The MO-Net model was implemented using TensorFlow API and training was carried out using a GPU cluster (GPU: Nvidia RTX 6000 with 24GB GPU memory). The training process took about 2.5 hours. The trained MO-Net was tested on remaining 316 images. An accuracy of 0.76±0.11 was achieved for the segmentation of leads and coils and it was measured in DSC against the ground truth. Although the MO-Net is not always able to detect the completed length of leads, it is sufficient for our next task: extracting geometric features. More importantly, the recall of coils is 1.0 and it means that all coils within X-ray images have been successfully detected as the coils are high-contrast objects and relatively easy to be detected. Secondly, the accuracy of the tip region detection for the pacing lead is measured by IoU. An accuracy of 0.82±0.07 was achieved. An example of segmentation results and lead tip detection inside the RV are presented in figure 7.

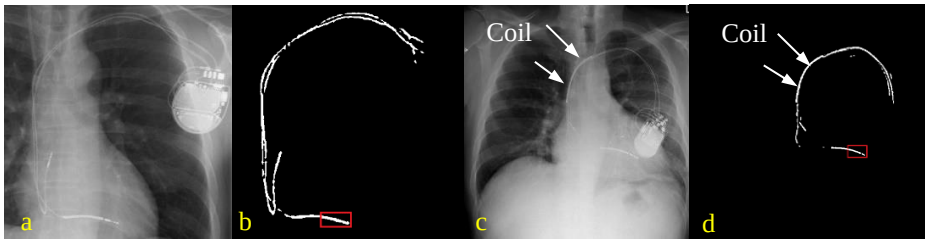

Fig. 7. The results of detecting leads and coils. (a)(c) The original image. (b)(d) The segmentation results output and lead tip detection output by the MO-Net. (c) The coil is clearly within the detected segmentations.

2.4 The detection of coils

Although the previous segmentation results already include the pacing leads and coils, the coils have not been detected as separate objects. Determining the coil's placement relative to the SVC is essential for evaluating the risks associated with TLE procedures. [10] reported that the fibrotic tissue surrounding the coil is one of leading factors contributing to the mechanical damages such as tear during the procedure. To detect only the coil, a standard U-Net model is used and the input image is an image mask, which is generated from the previous segmentation results. An image dilation operation with the kernel size of 10x10 were applied on the binary images [11], which were the previous segmentation results for pacing leads and coils. Finally, the dilated binary images

were applied on the original images to generate the masked images and they were used as the input images for the U-Net model.

To reduce the distraction from the thin lead wires, the input images were down-sampled to 256x256 before inputting them into the U-Net model. The same data augmentation technique was applied to the training images. The contrast or brightness of the 737 images were reduced by a random factor between 0.6 to 0.9 to create additional 1,474 training images. Therefore, total 2,211 training images were created. The trained U-Net was tested on remaining 316 images. An accuracy of 0.87±0.10 was achieved for the detection of coils and it was measured in DSC against the ground truth. To measure the performance of U-Net with or without data augmentation, key metrics such as accuracy, precision, recall and F1-score were calculated and presented in table 2. A true positive detection is defined as at least 75% length of the target coil object was detected. A false positive detection is defined as the other wire object was detected as the target coil object. An example of coil segmentation is presented in figure 8.

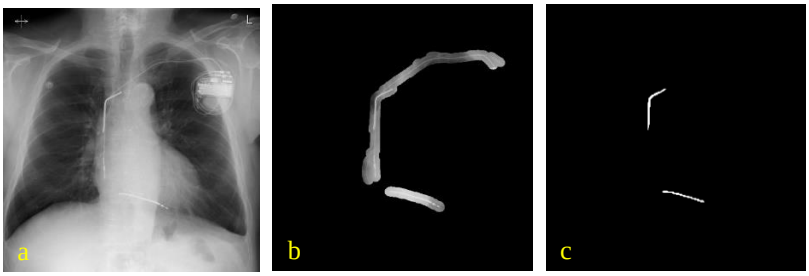

Fig. 8. An example of coil detection. (a) The original image. (b) The masked image. (c) The segmentation of only coils.

Table 2. Results of precisions and recalls.

Data augmentation	Accuracy	Precision	Recall	F1 score
without	0.88	0.89	0.92	0.90
with	0.98	0.98	0.99	0.98

3 The Extraction of Geometric Features

The geometric features are the lead coil position related to the superior vena cava (SVC), the lead angulations at different locations and the number of overlapping leads in the SVC.

3.1 The determination of the coil position related to the SVC

To quantify the exact location of the detected coil, the centerline extract method described in [9] was used. As illustrated in figure 9a, the binarized image of detected coils has been skeletonized so that the centerlines are represented as one-pixel-wide objects. Then a contour finding algorithm [12] was used to extract an array of 2D points of the

centerlines. The 2D points were sorted along the long axis of the bounding box of the SVC (the green box in figure 9a). By comparing the array of 2D points and the bounding box of the SVC, we can work out the percentage of the coil inside the SVC.

3.2 The lead angulations

There are two lead angulations could contribute to the tissue damage during the TLE procedures [13]. As illustrated in figure 9b, one is the angulation (highlighted in red) near the entry point of the SVC. The other is the angulation (highlighted in green) within the RV. When any of those two angles become acute, it could increase the risk. The acute angle is the angle of less than 90 degree.

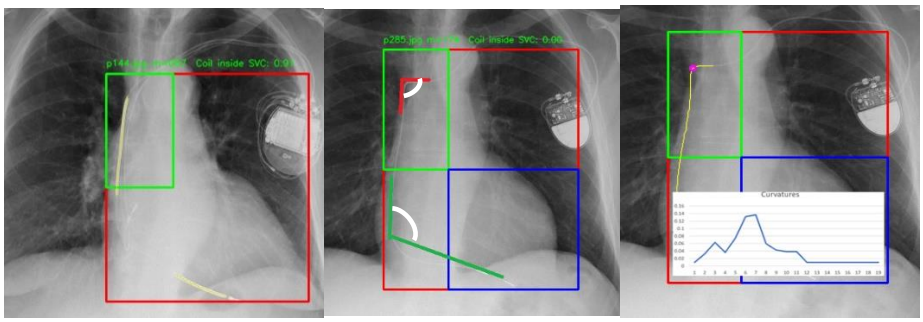

(a) (b) (c)

Fig. 9. (a)The workflow of the determination of the coil position related to the SVC. (b) Lead angulations. (c) Find the turning point.

The angulation near the entry point of the SVC. In order to compute the angle, the turning point need to be located first. This can be done by computing the local curvature estimation. To compute the local curvature efficiently, an approximation method was developed. In mathematics, the local curvature is defined as *1/R*, where *R* is the radius of an approximation circle which is fitted with the curve. As shown in figure 10, the approximation circle touches the curve on the point where the local curvature calculation is required. Assume that that Pt_1 and Pt_2 are both on the approximation circle and the curve. Therefore, $R = 0.5C/sin\alpha$. As $\alpha + \beta = 90^{\circ}$, $sin\alpha = \cos\beta$. the equation can be rewritten as $R = 0.5C/cos\beta$. To compute $cos\beta$, the dot product of vector V_1 and V_2 should be used. The relationship is $cos2\beta = \overrightarrow{V_1} \cdot \overrightarrow{V_2} / \|\overrightarrow{V_1}\| \|\overrightarrow{V_2}\| = 2cos^2\beta - 1$. Finally, local curvature can be computed as $Curv = 1/R = \sqrt{(\overrightarrow{V_1} \cdot \overrightarrow{V_2} / \|\overrightarrow{V_1}\| \|\overrightarrow{V_2}\| + 1)/2}/0.5C$. Finally, the turning point is where the local curvature reaches the maximum level. The angulation was calculated by using two vectors (one from each side). Each vector is located where the local curvature reaches a local minimum. Figure 9c show an example of the computation of the local curvatures and the detected turning point.

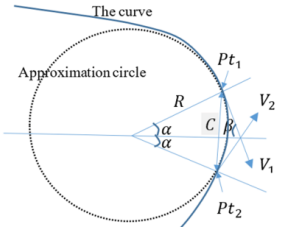

Fig. 10. Illustration for local curvature approximation.

The definitions of lead angulations. The angulation of the pacing lead in the RV is relatively easy to compute, which is defined as the angle between two vectors. One is the direction vector for the pacing lead coming out of the SVC and the other one is the direction vector for lead tip, which can be computed from the second output from MO-Net. In order to increase the robustness, the principal component analysis (PCA) was performed on the wire data to generate the direction vectors [14].

The results. The proposed methods for detecting acute angles were tested on all 1,053 chest X-ray images. The ground truth was the manual labelling of acute angles in two positions: the entry point of the SVC and inside the RV. The manual labels were created by a clinical expert. In the manual labels, there are 143 images with an acute angle inside the RV and only 7 images with an acute angle near the entry point of the SVC. To measure the performance of proposed methods, key metrics such as accuracy, precision, recall and F1-score were calculated and presented in table 3.

Table 3. Key metrics for the performance of acute-angle detection methods.

Location	Accuracy	Precision	Recall	F1 score
SVC	0.70	0.83	0.71	0.77
RV	0.91	0.97	0.92	0.95

3.3 Detecting the number of leads in the SVC

As the common reason for the major complication inside the SVC is the fibrotic tissue around the lead or the coil, it is also necessary to determine the approximate number of leads inside the SVC. A coil or more than two leads detected inside the SVC is considered as the risk factor for TLE procedures [10]. It is not possible to determine the exact number of leads inside the SVC robustly due to leads quite often overlaps each other and group together. Therefore, one way of determining the risk factor is whether more than two leads inside the SVC or not (the standard pacemaker has only two leads). The other way is whether 50% coil is within the SVC. To count the number of leads inside the SVC, the lead segmentation from the first output of MO-Net was binarized first and the centerlines were localized using the method in [9]. Running a line scanning algorithm within the bounding box of the SVC to count how many leads are inside the SVC. The detection method was tested on 809 chest X-ray images, which do not have a coil inside the SVC. The ground truth was the binary label for each image. There are 61 images (out of 809 images) with the binary label set to true by a clinical expert if there

are more than 2 leads inside the SVC. The performance metrics of accuracy, precision, recall and F1-score of the detection method are 0.782, 0.879. 0.836 and 0.857, respectively.

4 Feature Selection and Machine Learning Model

4.1 Feature selection

There are several geometric features suggested by the senior clinician and the values of those features generated by the detection algorithms are binary values. Therefore, the Jaccard similarity coefficient (JSC) [15] was used to test the correlation between individual geometric feature and the binary outcome of procedure complication, as the JSC is a statistical measure for correlating the similarity between binary data samples. However, JSC cannot be directly applied to our highly imbalanced data. In our data, 97.6% of sampling data are in the majority class, with only 2.4% of the sampling data in the minority class (major complication cases). Therefore, the imbalanced ratio is 40.7:1. Highly imbalanced data could distort the results of the correlation tests towards the majority class [16]. To balance the test data, Adaptive Synthetic (ADASYN) sampling techniques [17] were used. As shown in table 4, the feature of acute angle near the entry point of the SVC has the lowest JSC score and the detection method for that feature is also not robust (recall is just 0.714). Therefore, it was removed from the feature list.

Table 4. The results of the JSC tests.

Geometric Features	JSC Score
50% of coil or >2 leads inside the SVC	0.351
The acute angle inside the RV	0.029
The acute angle near the entry point of the SVC	0.005

4.2 Machine learning model for risk assessment

Once the geometric features were selected, they were combined with personal health data to feed into a machine learning model to predict the TLE procedure risk. The personal health data includes gender, age, history of heart failure, respiratory disease status, heart ejection fraction, and other relevant information. The XGBoost classifier [18] was chosen to predict the risk of TLE procedures as because it works well with imbalance datasets and binary classifications [19]. There are total 1053 sets of data from 1,053 TLE clinical cases and the outcome from 25 cases (2.4%) are a major complication or procedure related death. To balance the data, ADASYN were applied to the data and generated additional 1,003 sets of data which was labelled as the cases of a major complication or procedure related death. The balanced data were split into two groups. 70% of data were used for training and 30% of data were used for testing.

In order to compare the performance of model prediction, the XGBoost classifier was trained on the data related to personal health data and geometric features. Geometric features were detected by our computer vision algorithms. Those datasets were used

for training and testing the XGBoost classifier. After the training, the model prediction is assessed on the test data only. As shown in table 5, the balanced accuracy of model prediction using geometric features has improved substantially, when compared with the model prediction without using any of geometric features. Finally, the ranking of feature importance was shown in figure 11.

Table 5. The results of the model prediction. AUC is the area under curve.

Geometric features	Accuracy	Recall (major)	Recall (minor)	F1 score	AUC
Without	0.74	0.82	0.62	0.73	0.77
with	0.91	0.91	0.88	0.90	0.96

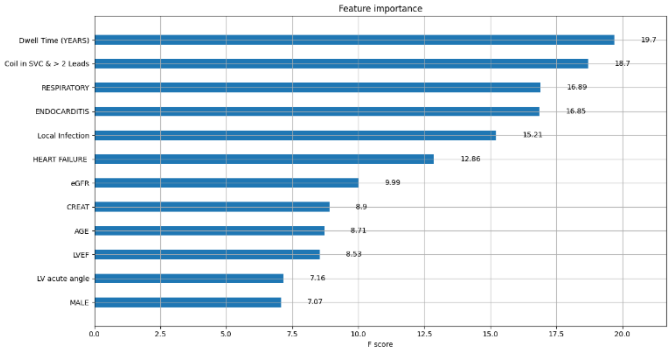

Fig. 11. Feature importance. There are two geometric features in the list: "Coil in SVC & >2 leads" and "RV acute angle".

5 Conclusions

This paper presents a novel deep-learning framework for predicting the risk of the TLE procedures. Robust deep-learning methods were developed to extract geometric features from plain chest X-ray images and the selection of geometric features was carried out by using the statistical analysis. By combining the geometric features with the personal health data, we were able to achieve a higher classification accuracy for detecting high-risk cases in the TLE procedures. The proposed framework not only has substantially improved the chance to identify the high-risk patients but also reduce the chance of falsely identifying low-risk patients as high-risk patients. Our approach only use plain chest X-ray images as the additional data source and the chest X-ray images are routinely acquired before the TLE procedures. Therefore, our approach does not require additional data and will not change current clinical practices for the TLE procedures. The results have demonstrated "lead dwell time" and "coil & more than 2 leads in SVC" were primary features predicting major complication cases in the XGBoost classifier (figure 11). This supports current clinical guidance and suggests clinical judgement remains paramount in appropriate patient risk stratification.

Our methodology for feature extraction, feature selection and model building is not limited to the risk prediction of the TLE procedures. The same methodology could be applied to other high-risk cardiac interventional procedures as well as applied to other commonly used medical images such as CT images or X-ray fluoroscopic images.

6 Acknowledgement

This work is funded by a EPSRC grant (EP/X023826/1). The study was also supported by the Wellcome/EPSRC Centre for Medical Engineering (WT203148/Z/16/Z) and the National Institute for Health Research (NIHR) Biomedical Research Centre based at Guy's and St Thomas' NHS Foundation Trust and King's College London. The views expressed are those of the author(s) and not necessarily those of the NHS, the NIHR or the Department of Health.

References

1. van Erven et al.: Attitude towards redundant leads and the practice of lead extractions: a European survey. Europace 12(2), 275–276 (2010).
2. Bongiorni, M. G., et al.: The European Lead Extraction ConTRolled (ELECTRa) study: A European Heart Rhythm Association (EHRA) Registry of Transvenous Lead Extraction Outcomes. European Heart Journal 38(40), 2995–3005 (2017).
3. Sidhu, B. S., et al: Risk stratification of patients undergoing transvenous lead extraction with the ELECTRa Registry Outcome Score (EROS): an ESC EHRA EORP European lead extraction ConTRolled ELECTRa registry analysis. Europace 23(9), 1462–1471 (2021).
4. Mehta, V. S., et al.: Machine learning–derived major adverse event prediction of pa-tients undergoing transvenous lead extraction: Using the ESC EHRA EORP European lead extraction ConTRolled ELECTRa registry. Heart Rhythm 19(6), 885-893 (2022).
5. Tułecki, Ł., et al.: A Study of Major and Minor Complications of 1500 Transvenous Lead Extraction Procedures Performed with Optimal Safety at Two High-Volume Re-ferral Centers. International journal of environmental research and public health 18(19), 10416-29 (2021).
6. Tariq M, Palade V, Ma Y, Altahhan A.: Diabetic retinopathy detection using transfer and reinforcement learning with effective image preprocessing and data augmentation techniques. Fusion of machine learning paradigms: theory and applications, Springer, Cham., 236, 33–61 (2023).
7. Chest X-Ray Image database, https://www.kaggle.com/datasets/paultimothymooney/chest-xray-pneumonia
8. Ma, Y. et al.: A Tensor-Based Catheter and Wire Detection and Tracking Framework and Its Clinical Applications. IEEE transaction on Biomedical Engineering, 69(2), 635–644 (2022).
9. Ma Y., Alhrishy M., Narayan S.A., Mountney P., Rhode K.S.: A novel real-time com-putational framework for detecting catheters and rigid guidewires in cardiac catheterization procedures. Medical Physics, 45(11), 5066–5079 (2018).
10. Tułecki, Ł., et al.: Analysis of Risk Factors for Major Complications of 1500 Transvenous Lead Extraction Procedures with Especial Attention to Tricuspid Valve Damage. International journal of environmental research and public health 18(17), 9100-9113 (2021).

11. Ma, Y., Mehta, V.S., Rinaldi, C.A., Hu, P., Niederer, S., Razavi, R.: Automatic Detection of Coil Position in the Chest X-ray Images for Assessing the Risks of Lead Extraction. FIMH 2023. LNCS, vol 13958. Springer, Cham (2023).
12. Wu X., Housden J., Ma Y., Razavi B., Rhode K. and Rueckert D.: Fast Catheter Segmentation From Echocardiographic Sequences Based on Segmentation From Corresponding X-Ray Fluoroscopy for Cardiac Catheterization Interventions. IEEE Transactions on Medical Imaging, 34(4), 861-876 (2015).
13. Bashir J., et al.: Classification and Surgical Repair of Injuries Sustained During Transvenous Lead Extraction. Circulation: Arrhythmia and Electrophysiology, 9(9), (2016).
14. Panayiotou M., et al.: A statistical method for retrospective cardiac and respiratory motion gating of interventional cardiac x-ray images. Medical Physics, 41, 071901, 1-13 (2014).
15. Chung N., et al..: Jaccard/Tanimoto similarity test and estimation methods for biological presence-absence data. BMC Bioinformatics, 20(644), (2019).
16. Lai C., et al.: A robust correlation analysis framework for imbalanced and dichotomous data with uncertainty. Information Sciences, 470, 58-77 (2019).
17. He H., et al.: ADASYN: Adaptive synthetic sampling approach for imbalanced learning. IEEE International Joint Conference on Neural Networks, 1322-1328 (2008).
18. Chen, T., et al.: XGBoost: A Scalable Tree Boosting System. Proceedings of the 22nd ACM SIGKDD International Conference on Knowledge Discovery and Data Mining (KDD '16), 785–794. (2016).
19. Ogunleye, A., et al.: XGBoost Model for Chronic Kidney Disease Diagnosis. IEEE/ACM Transactions on Computational Biology and Bioinformatics 17(6), 2131-2140 (2020).